The Astrophysical Journal, 762:84 (8pp), 2013 January 10 doi:10.1088/0004-637X/762/2/84

THE CHROMOSPHERIC SOLAR MILLIMETER-WAVE CAVITY ORIGINATES IN THE TEMPERATURE MINIMUM REGION

Victor De la Luz[1,2], Jean-Pierre Raulin[3], and Alejandro Lara[2]
[1] Instituto Nacional de Astrofisica, Optica y Electronica, Tonantzintla, Puebla, Mexico, Apdo. Postal 51 y 216, 72000, Mexico
[2] Instituto de Geofísica, Universidad Nacional Autónoma de México, México 04510, Mexico
[3] CRAAM, Universidade Presbiteriana Mackenzie, São Paulo, SP 01302-907, Brazil
Received 2012 February 17; accepted 2012 November 7; published 2012 December 18

ABSTRACT

We present a detailed theoretical analysis of the local radio emission at the lower part of the solar atmosphere. To accomplish this, we have used a numerical code to simulate the emission and transport of high-frequency electromagnetic waves from 2 GHz up to 10 THz. As initial conditions, we used VALC, SEL05, and C7 solar chromospheric models. In this way, the generated synthetic spectra allow us to study the local emission and absorption processes with high resolution in both altitude and frequency. Associated with the temperature minimum predicted by these models, we found that the local optical depth at millimeter wavelengths remains constant, producing an optically thin layer that is surrounded by two layers of high local emission. We call this structure the Chromospheric Solar Millimeter-wave Cavity (CSMC). The temperature profile, which features temperature minimum layers and a subsequent temperature rise, produces the CSMC phenomenon. The CSMC shows the complexity of the relation between the theoretical temperature profile and the observed brightness temperature and may help us to understand the dispersion of the observed brightness temperature in the millimeter wavelength range.

Key words: methods: numerical – radiation mechanisms: thermal – radiative transfer – stars: chromospheres – Sun: chromosphere – Sun: radio radiation

Online-only material: color figures

1. INTRODUCTION

The necessity of a two-component (hot and cold) model to explain chromospheric solar observations was established by Giovanelli (1949). A low-temperature zone in the chromosphere was inferred by observations in different regions of the solar spectrum in both line-emission (e.g., H and K of Ca II in the visible; Mg *h* and *k* resonance lines in the UV) and continuum (e.g., the 135–168 nm in UV and the 33–500 μm in microwave ranges). Moreover, by observing emission lines (Fe, Si, *K1* of Ca II, and *k1* of Mg) at the disk center, the height of the low-temperature region was set at the lower part of the chromosphere, very close to the photosphere (Athay 1970).

A considerable advance in the understanding of the chromosphere was obtained by the so-called VAL models. Using these models and based on adequate spatial resolution observations, Vernazza et al. (1973, 1976, 1981) found that a minimum temperature can be modeled by assuming a plane-parallel atmosphere in hydrostatic equilibrium and considering non-local thermodynamic equilibrium (NLTE). After that, Fontenla et al. (1990) improved the VAL models by including several updates (both observationally and theoretically), the most important being the ambipolar diffusion which removed the "plateau" of temperature in the high chromosphere.

The most recent and advanced model is the so-called C7 model (Avrett & Loeser 2008), which also follows the common assumptions of Vernazza et al. (1973). In particular, this model predicts that the continuum emission at 500 μm comes from the region where the temperature reaches its minimum value. The temperature minimum region has been set by the mentioned semi-empirical models at heights ranging between 400 and 600 km above the photosphere (Kuznetsova 1978; Ahmad & Kundu 1981; Vernazza et al. 1981; Fontenla et al. 1990; Avrett & Loeser 2008). In the literature, we also found purely empirical models, for example, the SEL05 model (Selhorst et al. 2005), which closely matches the observations made by Ewell et al. (1993), Kuseski & Swanson (1976), Beckman et al. (1973), and Linsky (1973).

Despite the fact that the chromosphere (where the temperature reaches minimum) plays a fundamental role in the dynamics and heating of the upper atmosphere (acting as the interface between the lower photospheric layers where β, the ratio between the dynamic and magnetic pressures, is much higher than one and the higher dynamic atmosphere where $\beta \ll 1$), this layer is not well understood. Recently, a renewed interest on this fundamental layer has grown due to the advent of better observational and reconstruction techniques applied to ground-based as well as spaceborne telescopes that have provided access to high space and time resolution observations of the solar chromosphere.

In this context, the analysis of the aforementioned models predicts that the millimeter and submillimeter (7.5–0.75 mm) quiescent solar emission comes from a layer in the lower chromosphere related to the minimum temperature (Vernazza et al. 1981).

It is well established that the height and width of a radio-emitting layer can be characterized using radiative transport models (Avrett & Loeser 2008). However, in general, these analyses consider only the upper layer (or final boundary) of the emission region, i.e., the layer where the atmosphere becomes optically thick. Therefore, the knowledge and understanding of the local emission produced at lower layers remains neglected. Note that the fact that these regions are not easily accessible to radio telescopes does not prevent us from studying the possible physical processes occurring inside them. To overcome these limitations, in a previous analysis of the quiet chromosphere, we

explored the local emission at 17, 212, and 405 GHz frequencies and found that there are two main regions of emission; the first one is close to the photosphere and the second is located at ~1000 km over the photosphere (De la Luz et al. 2011).

In the present work, we continue to study the local radiative transfer processes in different layers of the atmosphere (we present a brief description of the model in Section 2; for details see De la Luz et al. 2011) for the empirical model SEL05 and two semi-empirical models, C7 and VALC (Section 3), but extend our study to a larger range of frequencies from 2 GHz to 10 THz (Section 4). In particular, we study the radio emission associated with the minimum temperature and the lower chromosphere (Section 5).

It is worth mentioning that the study of the solar spectrum morphology, especially at submillimeter and infrared wavelengths, is also important for studies of dusty circumstellar disks (Zuckerman 2001) because the emission from the chromosphere of main-sequence solar-like stars at these wavelengths could be comparable to that emerging from circumstellar material.

2. RADIO EMISSION MODEL

In order to compute the radio emission, we solve the local radiative transfer equation. The amount of energy dI_ν passing through the volume element characterized by the length ds is equal to the absorption $I_\nu\kappa_\nu$ plus the emission ϵ_ν inside the element, which is

$$\frac{dI_\nu}{ds} = -I_\nu\kappa_\nu + \epsilon_\nu, \tag{1}$$

where κ_ν is the opacity function and ϵ_ν is the emission function. The solution of the radiative transfer equation can be represented in a local cell as follows:

$$I_{\rm lcl} = \epsilon_{\rm abs} + \epsilon_{\rm emi}, \tag{2}$$

where $I_{\rm lcl}$ is also known as the contribution function (Gray 1976), and

$$\epsilon_{\rm abs} = I_0 \exp(-\tau_{\rm lcl}) \tag{3}$$

is the local absorption and

$$\epsilon_{\rm emi} = S_{\rm lcl}(1 - \exp(-\tau_{\rm lcl})) \tag{4}$$

is the local emissivity. In this case, I_0 is the incoming radiation, $\tau_{\rm lcl}$ is the local optical depth, and $S_{\rm lcl}$ is the local source function. We remind the reader that the specific intensity, I_ν, can be converted to brightness temperature, T_b, using the Rayleigh–Jeans approximation:

$$I_\nu = \frac{2k\nu^2 T_b}{c^2}, \tag{5}$$

where c is the speed of light and k is the Boltzmann constant. Then we can rewrite Equation (2) using

$$T_{\rm blcl} = \frac{I_{\rm lcl}c^2}{2k\nu^2}, \tag{6}$$

where $T_{\rm blcl}$ is the local brightness temperature.

In order to characterize the local efficiency emission and absorption of the atmosphere, we define

$$E_l = 1 - \exp(-\tau_{\rm lcl}) \tag{7}$$

as the local efficiency of emissivity and

$$A_l = \exp(-\tau_{\rm lcl}) \tag{8}$$

as the local efficiency of absorbance. The values for E_l and A_l can vary between 0 and 1, where 0 means optically thin and 1 is optically thick.

Using the local emissivity and absorbance, we iteratively compute the emission over a ray path by solving the radiative transfer equation (De la Luz et al. 2010). Finally, the total emission efficiency, in the altitude range (ξ) from h_1 up to h_2, is

$$\epsilon_T(h_1, h_2) = 1 - \exp\left(-\sum_{\xi=h_1}^{h_2}\tau_{\rm lcl}(\xi)\right) = 1 - \exp(-\tau(h1, h2)), \tag{9}$$

where $\tau(h1, h2)$ is the optical depth between h_1 and h_2.

3. THE SOLAR CHROMOSPHERIC TEMPERATURE PROFILES

The temperature structure in the Sun, and in stars in general, decreases monotonically with stellar (solar) radius. In the case of the Sun, more elaborate models that include chromospheric heating (Vernazza et al. 1981; Selhorst et al. 2005; Avrett & Loeser 2008; VALC, SEL05, and C7 models, respectively) indicate that the temperature reaches a minimum value at about 400 and 600 km above the solar photosphere (Figure 1). Above this point, the temperature gradually increases up to coronal temperatures (≈1 MK).

A comparison among the three above-mentioned models shows only marginal differences in the temperature profile, but quite significant discrepancies at greater heights, including the value of the temperature minimum. For instance, the VALC model predicts that the temperature at the minimum ($T_{\rm min}$) is 4170 K and is located at 515 km above the photosphere. Similarly the models C7 and SEL05 place the minima at 560 ($T_{\rm min}$ = 4400 K) and 500 km ($T_{\rm min}$ = 4407 K), respectively.

By inspection of Figure 1, one can see that the results from the three models intersect at about 900 km. Above this point, the models behave differently. The SEL05 profile increases linearly with height until 7700 K, while the VALC model increases from 5800 to 7200 K but not linearly, C7 grows from 5800 to 6650 K which remains almost constant for the next 800 km. Finally, the VALC model presents a plateau in temperature (around 24500 K) between 2115 km and 2267 km.

In Figure 2, we plot the differences in the radial temperature profiles between the three models, taking the C7 model as a reference. We found three heights where the differences in temperature are higher than 6%: around 400 km (6% in only the VALC model), 750 km (8.5%), and 1100 km (6%). In these cases, the differences with the C7 model are significant but always less than 10%.

4. SYNTHETIC SPECTRUM

We use PakalMPI (De la Luz et al. 2011), an updated version of the Pakal code (De la Luz et al. 2010) to compute a synthetic spectrum of the solar emission from millimeter to infrared wavelengths (from 2 GHz to 10 THz). PakalMPI solves the radiative transfer equation with NLTE conditions, in a three-dimensional geometry using a multiprocessor environment. As a model of emission, we use "Celestun," which includes three opacity functions in the continuum: bremsstrahlung (Rybicki &

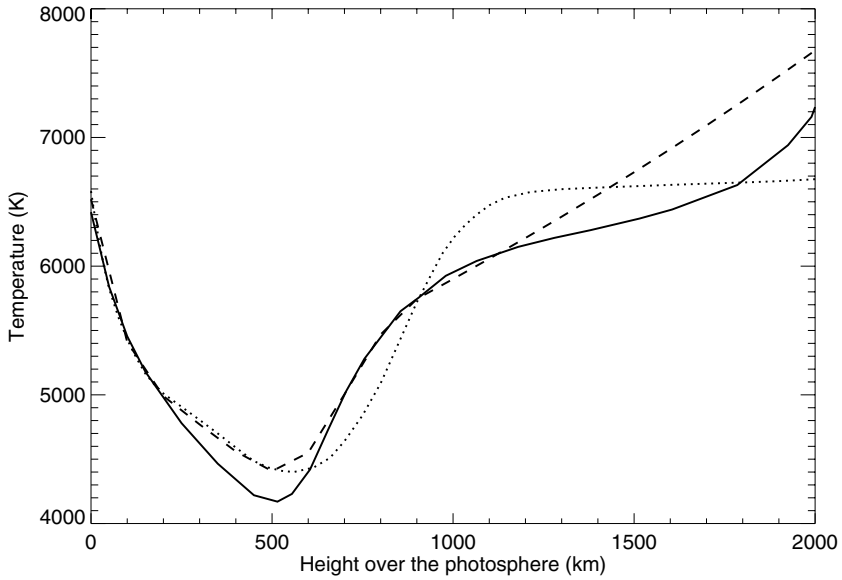

Figure 1. Radial temperature profiles of three chromospheric models. The continuous line is the VALC model from Vernazza et al. (1981), the dashed line corresponds to the model of Selhorst et al. (2005), and the dotted line is the C7 model from Avrett & Loeser (2008).

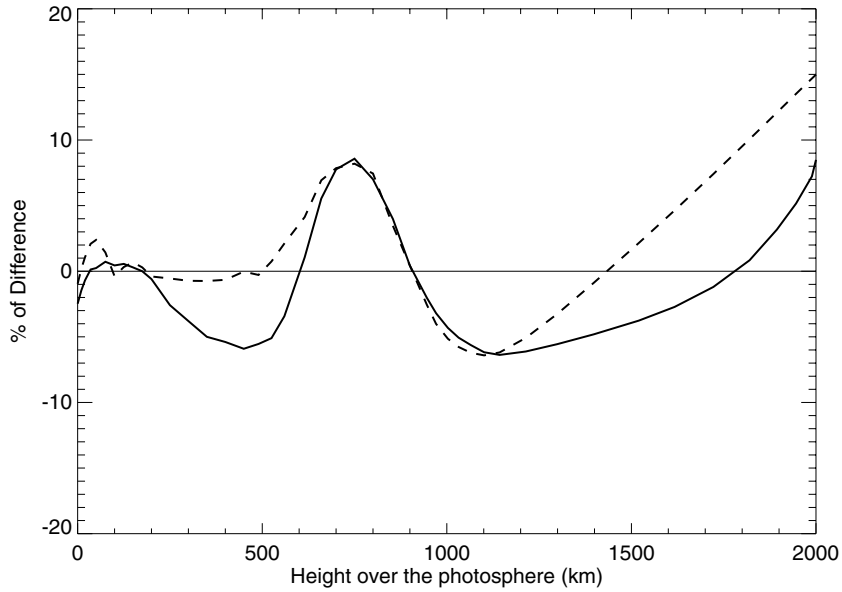

Figure 2. Difference in the temperature profile between the C7 model (taken as a reference), and the VALC (continuous line) and SEL05 (dashed line) models.

Lightman 1986), neutral interaction (John 1988; Zheleznyakov 1996), and inverse bremsstrahlung (Golovinskii & Zon 1980). The Celestun model also includes ionization stages of 20 ion species considering H, H^-, and n_e in NLTE (see De la Luz et al. 2011, for more details). The input parameters of PakalMPI are physical quantities such as temperature, hydrogen density, and metallicity. These parameters are taken from an atmospheric model, in this case the VALC, SEL05, and C7 models mentioned in the previous section.

In Figure 3, we show the differences between the final brightness temperature (synthetic spectrum) for the three models taking the C7 model as a reference. We show that below 90 GHz the differences between the C7 and the VALC models exceed 20%. A comparison between C7 and SEL05 shows differences of 30% or less in the entire frequency range under study, with the points in frequency being around 8, 200, and 1200 GHz which presents very similar brightness temperatures.

Figure 4 shows the computed optical depth (τ in Equation (9)) for each model at 10, 40, 200, and 800 GHz. For the C7 and the VALC models, between 480 and 1000 km over the photosphere (marked with vertical lines), the optical depth remains roughly constant. In other words, $\tau_{\rm lcl}$ is very small and the local emissivity is negligible (Equation (4)).

Using the SEL05 model, the local optical depth presents two steps in the same region. This is due to the fact that this model has an artificial peak enhancement of the hydrogen density which causes an increment of the opacity at ~600 km over the photosphere (Figure 5). This artificial peak also modifies the total and local efficiency. This region with hydrogen overdensity is a consequence of the fully ionized gas approximation used in the SEL05 model, which is not applicable at the low chromosphere (De la Luz et al. 2011).

Figure 6 shows the contour plot of the total emission efficiency (Equation (9)) as a function of frequency and height for

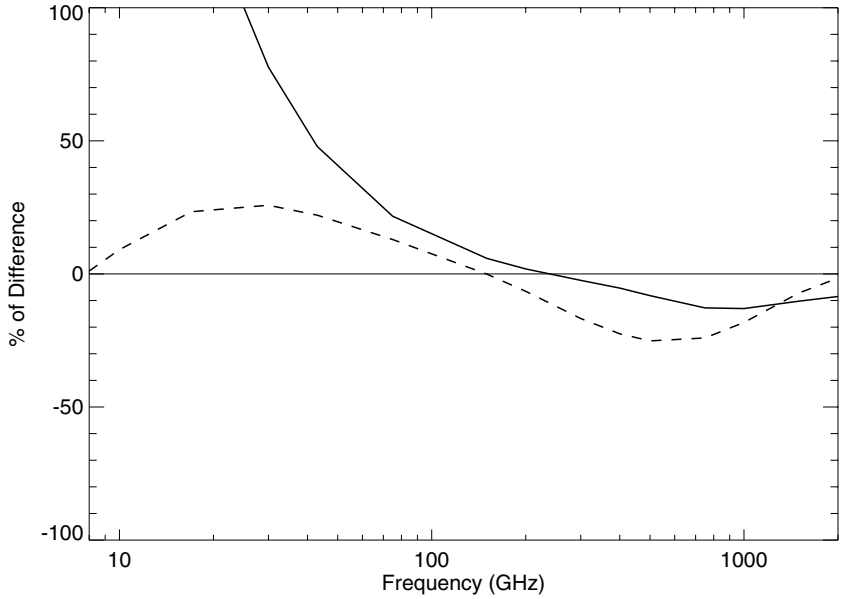

Figure 3. Difference in the brightness temperature between the C7 model (taken as a reference), and the VALC (continuous line) and SEL05 (dashed line) models.

the C7 model. In particular, we are interested in the interface between the optically thick and thin region (IOTT). The interface can be defined as the region in height where the emission efficiency is $0.9 > \epsilon_T > 0.1$.

This region is presented in the plot as the gradient ribbon between red (optically thick) and blue (optically thin) colors. We note that the final brightness temperature comes from the total optical depth and is related to the total emission efficiency. Analysis of the local emission and absorption process help us to understand the process although it remains hidden in observations.

In the case of the C7 model, one can see that the 10 GHz emission comes from a layer situated at about 2100 km above the photosphere, whereas the 100 GHz source is located at 1500 km above the photosphere. The IOTT in the 2–500 GHz frequency range is located in a large range of heights, between 1000 and 2100 km above the photosphere. On the other hand, inside the 500–2000 GHz frequency range, the IOTT remains roughly constant with altitude, from 500 to 1000 km. This is a direct consequence of the optical depth "plateau" shown in Figure 4.

The results for the VALC model are very similar to those obtained using the C7 model. We can see a slow decrease of the IOTT between 10 and 300 GHz, then an abrupt change around 400 GHz is observed.

At low frequencies, both the C7 and VALC models predict a very low, and therefore unrealistic, altitude of the emitting sources. This is due to the fact that these models do not take into account the corona and the transition region.

For the SEL05 model, the effect of the hydrogen overdensity in the emission efficiency is seen as a rapid shift of the IOTT toward higher frequencies at ∼600 km over the photosphere, where the peak of hydrogen is located (Figure 5). In this case, the inclusion of ad hoc coronal physical conditions produces an increment in the altitudes of the low-frequency sources (<30 GHz), giving more realistic results for this range of frequencies than the models without the corona (C7 and VALC models).

In Figure 5 from De la Luz et al. (2011), we can observe the brightness temperatures computed with these models and their comparison with the observations (collected by Loukitcheva et al. 2004). This figure shows that SEL05 provides the best match (although their approximation in the low chromosphere disagrees with the semi-empirical model predictions). The results of the C7 and VALC models present opposite behaviors. At lower frequencies, the predicted brightness temperature differs from the observations; C7 shows lower and VALC shows higher brightness temperatures in the same range of frequencies. This situation is partially inverted around 400 GHz where both models show a brightness temperature above that observed, but C7 predicts higher brightness temperatures than VALC. If we observe Figure 2, a direct relation between the differences in the radial temperature models and the final brightness temperatures cannot be easily established.

5. THE CHROMOSPHERIC MILLIMETER-WAVE CAVITY

De la Luz et al. (2010, 2011) reported that the emission profiles in the 40–400 GHz range have two regions of enhanced local emissivity. Remarkably, no attention has been paid to this interesting behavior. For instance, in Figure 2 from Avrett & Loeser (2008), we note that at 0.5 mm there are also two regions of emission; unfortunately, the authors did not elaborate on this result much. In this work, we present a detailed study of this region.

We show in Figure 7 the contour plot of the local emission efficiency (Equation (7)) as a function of frequency and height for the C7 model, where E_l varies from an optically thin (blue) to an optically thick (red) medium. There is a peculiar zone of low emissivity centered at about ∼750 km above the photosphere. This atmospheric zone forms a cavity starting at ∼40 GHz; its width grows with frequency and ends at ∼400 GHz.

Between 40 and 400 GHz the cavity, surrounded by two zones of enhanced local emission, is clearly seen. At a given frequency within this range (for instance 100 GHz), and moving outward from the photosphere, we first find a region where the atmosphere emits efficiently (in red color between 0 and 600 km), then there is a region where the atmosphere becomes thinner (in blue color between 600 and 900 km), and finally, a second region of emission appears (red color between 900 and 1300 km), i.e., we have crossed the local interface between

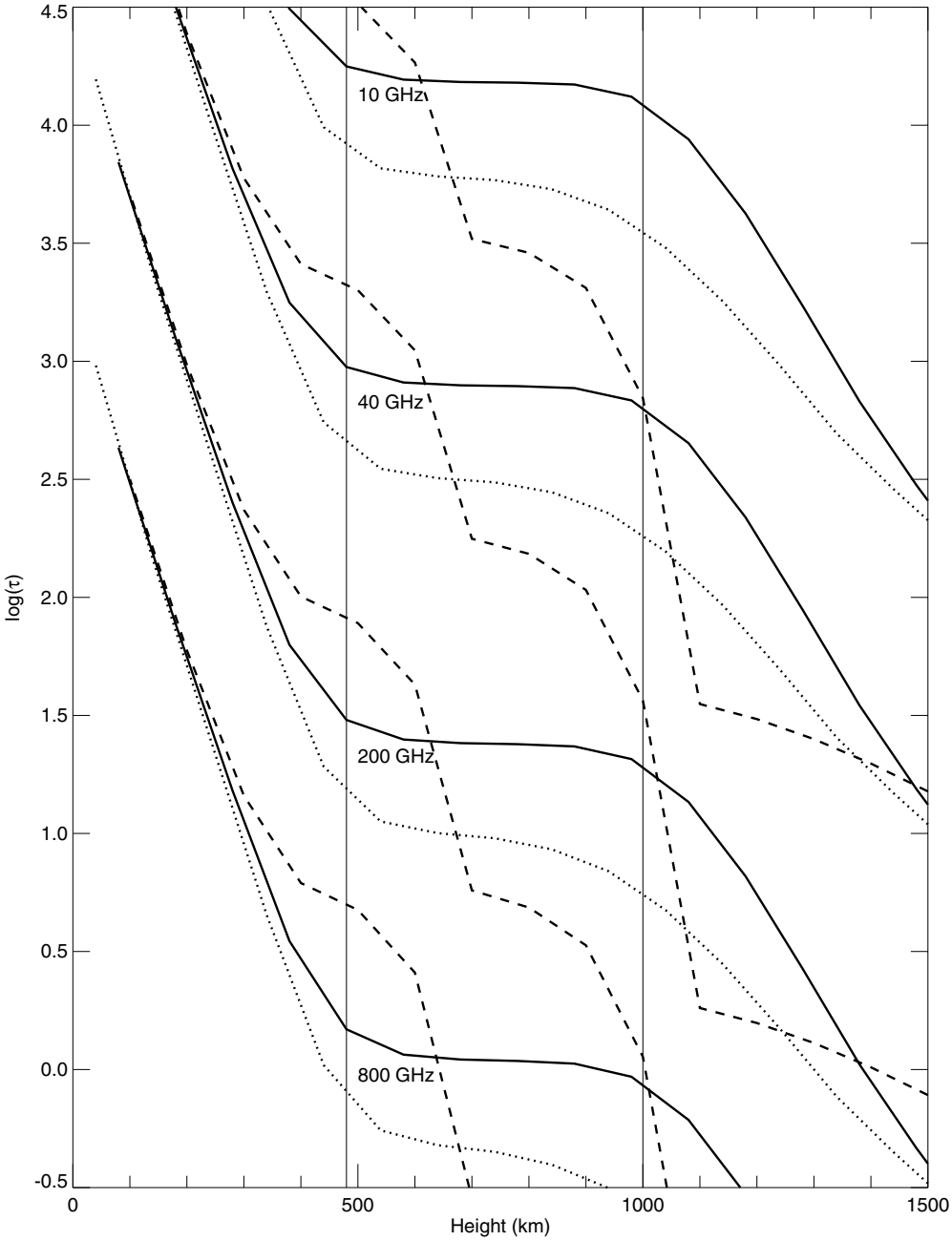

Figure 4. Optical depth computed for 10, 40, 200, and 800 GHz using the C7 (continuous line), VALC (dotted line), and SEL05 (dashed line) models. Note that the optical depth for the C7 and VALC models remains almost unalterable at heights between 480 and 1000 km over the photosphere, forming an optical depth plateau.

the optically thick and thin regions ($IOTT_l$) three times. In this case, $IOTT_l$ is defined as the region in height where the local efficiency of emissivity is $0.9 > E_l > 0.1$. The $IOTT_l$ divides the synthetic spectrum into three regions: between 2 and 40 GHz (where the $IOTT_l$ once is crossed), the second region between 40 and 400 GHz (crossed three times), and between 400 and 10,000 GHz (crossed once).

The VALC and SEL05 models show the same characteristic. The SEL05 model shows a more complex structure; in particular, it has a characteristic peak around 600 km over the photosphere, which has been discussed previously.

We call this region the Chromospheric Solar Millimeter-wave Cavity (CSMC). This is a region of the solar atmosphere where the opacity at millimeter and submillimeter wavelengths is reduced, surrounded by two zones of enhanced opacity. As far as we know, the presence of the CSMC has never been studied or previously mentioned in the literature.

6. DISCUSSION AND CONCLUSIONS

The optical thickness of the solar atmosphere depends on the opacity functions involved in the emission/absorption processes. At millimeter wavelengths, the important processes are the neutral interaction and the classical bremsstrahlung (De la Luz et al. 2011). These mechanisms depend on the temperature and the electronic and ion density.

In the chromospheric layers, close to the minimum temperature, the rate of ionization is low, and therefore the number of interactions between electrons and ions decreases, resulting in locally thin atmospheric layers (at millimeter wavelengths).

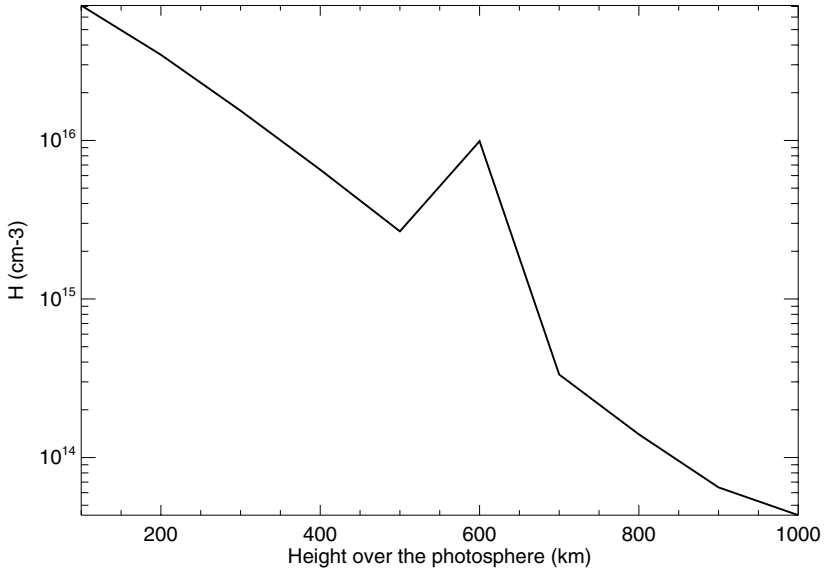

Figure 5. Hydrogen density profile from SEL05 model. The peak around 550 km is a consequence of the full ionized gas hypothesis.

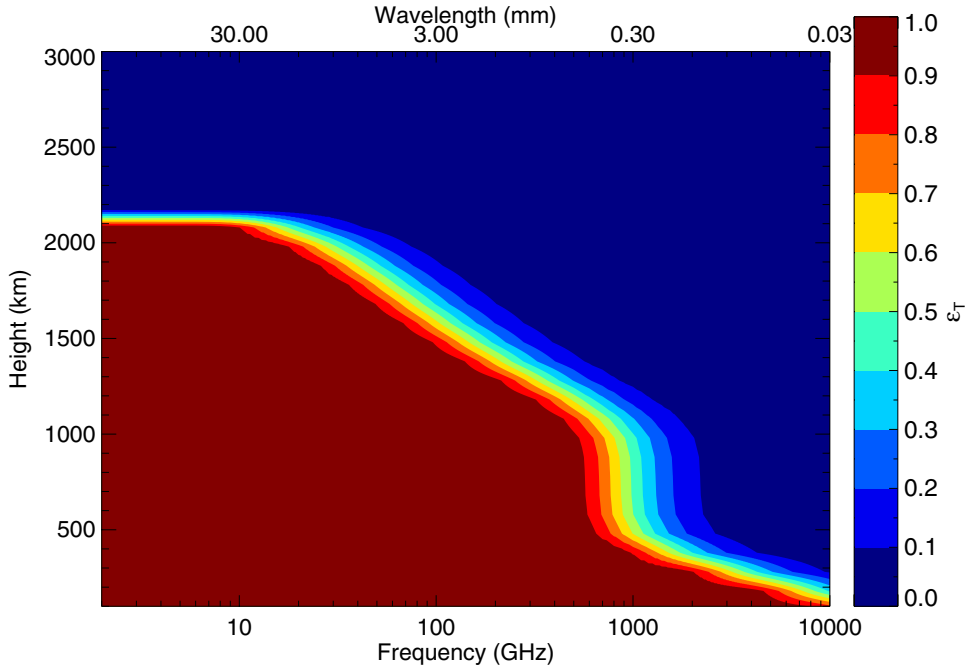

Figure 6. Synthetic solar spectrum from 2 GHz to 10 THz as a function of the atmospheric height over the photosphere. The contours correspond to the efficiency of the total emission (ϵ_T) computed using the C7 model (for this and the following figures blue means optically thin and red optically thick). The region between 500 and 200 GHz is an effect of the optical depth plateau.

(A color in the online journal version of this figure is available.)

Around this region, the temperature rises, producing free electrons and ions, and therefore these atmospheric layers become optically thick. The interplay between the optically thick and thin layers produces the CSMC.

We know (De la Luz et al. 2011) that in the first 500 km over the photosphere the neutral interaction is the most important mechanism in the emission and absorption process, and then bremsstrahlung becomes the major contributor in the optical depth. The second region of emission in the CSMC begins around 700 km over the photosphere, and we can conclude that the neutral interactions do not influence the resulting CSMC.

The morphology of the CSMC is a model-based phenomenon. In this work, we have used two well-known semi-empirical models (VALC and C7) and one ad hoc model (SEL05) and all of them showed the CSMC structure but with small changes in its morphology. We think that on average the models used reproduce the physical conditions in the low chromosphere well such that the computations in other regions of the spectrum show consistency (Vernazza et al. 1981; Avrett & Loeser 2008). However, the differences in the computed synthetic spectra at millimeter, submillimeter, and infrared regions should be taken into account not only to test the autoconsistence of the models but also as a tool to improve the radial temperature profile.

The presence of the CSMC shows that the relationship between the theoretical radial profile of temperature and the observed spectrum is complex, contrary to the general idea of a simple linear relationship as suggested by Avrett & Loeser (2008). We think that the CSMC must be an intrinsic

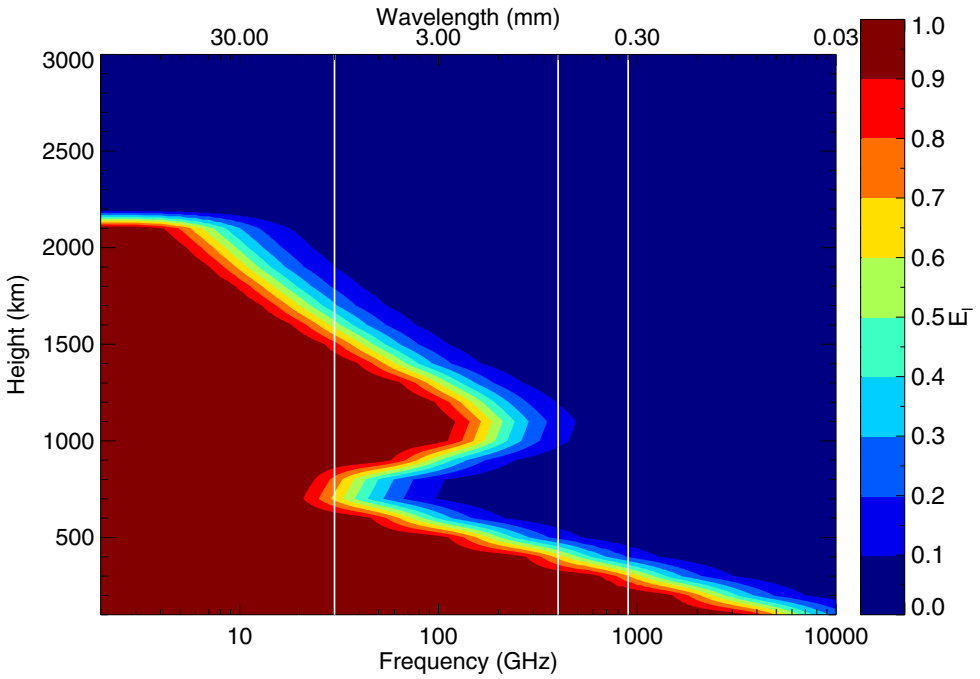

Figure 7. Contour plot of the local emissivity efficiency E_l computed using the C7 model, the white vertical lines mark the Chromospheric Solar Millimeter-wave Cavity (CSMC).

(A color in the online journal version of this figure is available.)

characteristic of the solar chromosphere and could help us to better understand the brightness temperature spectrum from the microwave to submillimeter range.

A comparison between the observations (collected by Loukitcheva et al. 2004) and the brightness temperature computed with C7 and VALC predicts higher brightness temperatures (Figure 5 from De la Luz et al. 2011) in almost the entire frequency range, except in the interval between 90 and 400 GHz. The SEL05 model better fixes the same observations, but in this work, we show that the SEL05 approximations cause inconsistencies in the hydrogen density profile.

The IOTT and the IOTT$_l$ define different frequency regions and heights of emission in the synthetic spectrum. The IOTT presents three regions—2–500 GHz, 500–2000 GHz, and 2000–10000 GHz—while IOTT$_l$ shows 2–40 GHz, 40–400 GHz, and 400–10000 GHz. Although the final brightness temperature is directly related to the IOTT, the true cause behind the shape spectrum is the IOTT$_l$, i.e., the CSMC.

We can conclude that to fix the high brightness temperature computed with C7 and VALC (after 400 GHz), we need to decrease the local optical depth around the heights of the second peak of local emission of the CSMC. The opacity function at these altitudes mainly depends on the bremsstrahlung process, i.e., lower temperatures than those published for C7 and VALC between 700 and 1500 km over the photosphere could decrease the local opacity values and then decrease the brightness temperature. In particular, we expect that the sources of emission more sensitive to the CSMC are at frequencies between 400 and 600 GHz, where the second peak of emission of the CSMC ends. We expect that the height of the source of emission may vary between 500 and 1000 km over the photosphere, causing a large dispersion in the spectrum at these frequencies.

On the low part of the spectrum, the inclusion of the transition region and corona could fix the low brightness temperatures predicted by C7 at frequencies lowers than 40 GHz. The VALC plateau of temperature between 2115 and 2267 km over the photosphere is responsible for the high brightness temperature computed with this model, in particular in the centimetric range. Submillimeter solar observations are needed in order to confirm the presence of the CSMC particularly between 400 and 600 GHz.

Finally, as the CSMC is a direct consequence of the minimum temperature layers (mostly of the gradual temperature rise in the low chromosphere), it could provide new insight into the structure of the solar atmosphere, and also it could be extended to the case of solar-like stars.

Part of this work was supported by UNAM-PAPPIT IN117309-3 and CONACyT 24879 grants. Thanks to the National Center of Super-computing in Mexico for allowing us to use their computer facilities and Dr. Emanuele Bertone and Dr. Miguel Chavez for useful comments. Thanks to Professor Pierre Kaufmann, director of CRAAM-Centro de Radioastronomia e Astrofisica Mackenzie, where part of this research was conducted. J.P.R. thanks the CNPq agency (Proc. 305655/2010-8).

REFERENCES

Ahmad, I. A., & Kundu, M. R. 1981, SoPh, 69, 273
Athay, R. G. 1970, ApJ, 161, 713
Avrett, E. H., & Loeser, R. 2008, ApJS, 175, 229
Beckman, J. E., Clark, C. D., & Ross, J. 1973, SoPh, 31, 319
De la Luz, V., Lara, A., Mendoza-Torres, J. E., & Selhorst, C. L. 2010, ApJS, 188, 437
De la Luz, V., Lara, A., & Raulin, J.-P. 2011, ApJ, 737, 1
Ewell, M. W., Jr., Zirin, H., Jensen, J. B., & Bastian, T. S. 1993, ApJ, 403, 426
Fontenla, J. M., Avrett, E. H., & Loeser, R. 1990, ApJ, 355, 700
Giovanelli, R. G. 1949, MNRAS, 109, 298
Golovinskii, P. A., & Zon, B. A. 1980, ZhTFi, 50, 1847
Gray, D. F. (ed.) 1976, The Observation and Analysis of Stellar Photospheres (New York: Wiley-Interscience)
John, T. L. 1988, A&A, 193, 189
Kuseski, R. A., & Swanson, P. N. 1976, SoPh, 48, 41
Kuznetsova, N. A. 1978, SvA, 22, 345

Linsky, J. L. 1973, SoPh, 28, 409
Loukitcheva, M., Solanki, S. K., Carlsson, M., & Stein, R. F. 2004, A&A, 419, 747
Rybicki, G. B., & Lightman, A. P. (ed.) 1986, Radiative Processes in Astrophysics (New York: Wiley), 400
Selhorst, C. L., Silva, A. V. R., & Costa, J. E. R. 2005, A&A, 433, 365
Vernazza, J. E., Avrett, E. H., & Loeser, R. 1973, ApJ, 184, 605
Vernazza, J. E., Avrett, E. H., & Loeser, R. 1976, ApJS, 30, 1
Vernazza, J. E., Avrett, E. H., & Loeser, R. 1981, ApJS, 45, 635
Zheleznyakov, V. V. (ed.) 1996, Radiation in Astrophysical Plasmas (Astrophysics and Space Science Library, Vol. 204; Berlin: Springer)
Zuckerman, B. 2001, ARA&A, 39, 549

The Astrophysical Journal, 802:142 (1pp), 2015 April 1 doi:10.1088/0004-637X/802/2/142

ERRATUM: "THE CHROMOSPHERIC SOLAR MILLIMETER-WAVE CAVITY ORIGINATES IN THE TEMPERATURE MINIMUM REGION" (2013, APJ, 762, 84)

Victor De la Luz[1], Jean-Pierre Raulin[2], and Alejandro Lara[3]
[1] SCiESMEX, Instituto de Geofisica, Unidad Michoacan, Universidad Nacional Autonoma de Mexico, Morelia, Michoacan, Mexico. CP 58190; vdelaluz@geofisica.unam.mx
[2] CRAAM, Universidade Presbiteriana Mackenzie, Sao Paulo, SP, 01302-907, Brazil
[3] Instituto de Geofisica, Universidad Nacional Autonoma de Mexico 04510, Mexico
Received 2015 January 17; accepted 2015 January 20; published 2015 April 2

In Figures 4 and 6, we found an incorrect scale for the optical depth (τ in Equation 9). We provide replacement figures with the corrected scale.

It does not affect the results and discussion in the published version of this paper.

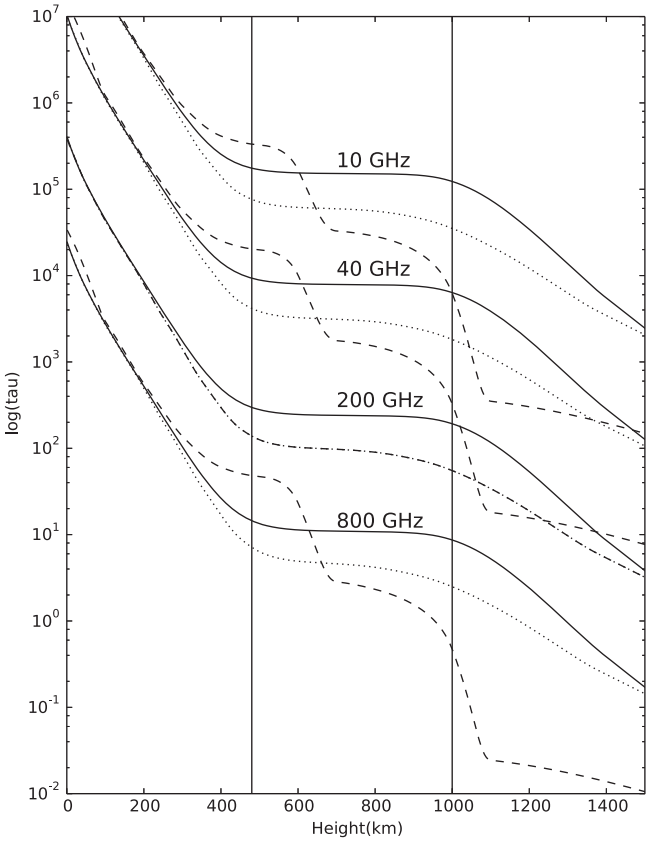

Figure 4. Optical depth computed for 10, 40, 200, and 800 GHz using the C7 (continuous line), VALC (dotted line), and SEL05 (dashed line) models. Note that the optical depth for the C7 and VALC models remains almost unalterable at heights between 480 and 1000 km over the photosphere, forming an optical depth plateau.

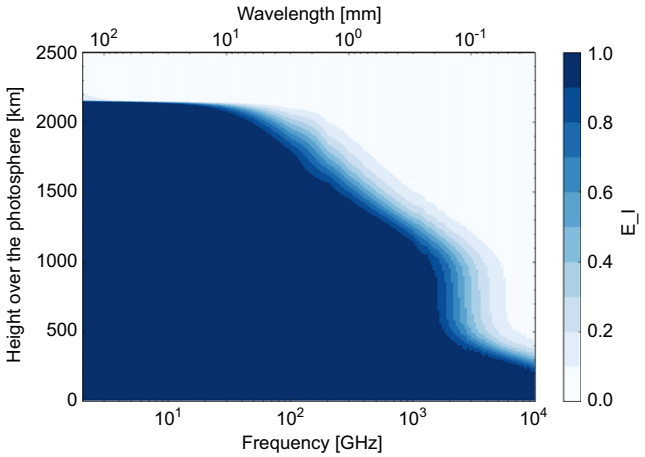

Figure 6. Synthetic solar spectrum from 2 GHz to 10 THz as a function of the atmospheric height over the photosphere. The contours correspond to the efficiency of the total emission (E_T) computed using the C7 model (blue means optically thick and white optically thin).